Comparison the performance of five-qubit IBM quantum computers in terms of Bell states preparation

Preprint · June 2020

CITATIONS
0

READS
16

1 author:

Mitali Sisodia
Indian Institute of Technology Jodhpur
15 PUBLICATIONS **137** CITATIONS

SEE PROFILE

Quantum Information Processing (2020) 19:215
https://doi.org/10.1007/s11128-020-02712-7

Comparison the performance of five-qubit IBM quantum computers in terms of Bell states preparation

Mitali Sisodia[1]

Received: 5 February 2020 / Accepted: 25 May 2020

Abstract
There are several quantum computing platforms available on cloud. In this paper, we have compared the performance of five-qubit superconductivity-based four IBM quantum computers, namely IBM_ourense, IBM_vigo, IBMQX2, IBMQX4. Specifically, we studied the Bell states preparation in all these cases. We have calculated the fidelity between the experimentally generated and theoretically prepared states to compare the performance of IBM quantum computers for all the Bell states. This comparison shows IBM_ourense quantum computer exhibits better performance than other (IBM_vigo, IBMQX2, IBMQX4) IBM quantum computers. This shows technological advancement as the newer platforms available on cloud perform better.

Keywords IBM quantum experience · Bell states preparation · Quantum state tomography

1 Introduction

There are several quantum information processing tasks have been done using various experimental platforms, such as an experimental architecture based on NMR, ion-trap, silicon, nitrogen-vacancy center ([1–8] and references therein). Among these experimental architectures based on experimental platforms, one experimental platform deserves the special attention which is released by IBM in 2016 a five-qubit universal quantum computer prototype accessible on the cloud, based on superconducting qubits: the IBM Quantum Experience (IBM QE) [9]. This experimental platform has attracted the attention of the entire quantum information community because everyone can access it freely and easily through IBM Quantum Experience. There are several multi-qubit IBM quantum computers, which is also made up of superconducting transmon qubits, i.e., five-qubit, 15-qubit, 16-qubit, 20-qubit. Interestingly, several quantum

✉ Mitali Sisodia
mitalisisodiyadc@gmail.com

[1] Indian Institute of Technology Jodhpur, Jodhpur, Rajasthan 342011, India

Published online: 15 June 2020

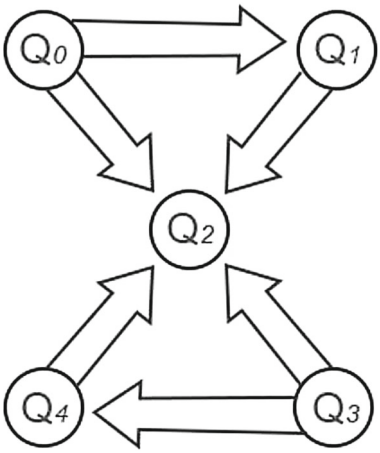

Fig. 1 Architecture of old IBMQX2 for CNOT gate. These arrows shows which qubits are connected or which are not. For example, Q_4 and Q_0 are not connected, so CNOT gate can not be applied between these two qubits

communication tasks [10–25] have already been verified and tested of Leggett–Garg [26] and Mermin inequality [10], non-Abelian braiding of surface code defects [15], entropic uncertainty and measurement reversibility [27], Hardy's paradox [28], topological quantum walks [29], quantum permutation algorithm [30] and entanglement assisted invariance [31] have been illustrated by using these SQUID-based quantum computers. But five-qubit IBM quantum computer is the world's first commercial quantum computing service provided by IBM corporation via. a free web based interface called IBM Quantum Experience (IBM QE) [9] for the users. A proper advantage of it taken by researchers by demonstrating and running a variety of quantum computing experiments, e.g., [10–17,20,28,29,32]. In the old (which is placed in cloud in 2016) five-qubit IBM quantum computers i.e. IBMQX2 and IBMQX4, the set of quantum gates Hadamard gate (H), the Pauli gates X, Y, Z phase gates S, $S^\dagger$, $\frac{\pi}{4}$ gates T, $T^\dagger$, as well as the entangled two-qubit controlled-NOT (CNOT) gate were available. Users were free to apply single qubit quantum gates anywhere on the qubit lines. However, two-qubit CNOT gate could not apply anywhere, it had some restrictions. CNOT gate could apply only according to the architecture (topology) as shown in Fig. 1 as an example of the topology of CNOT gate.

Due to these restrictions and unavailability of two and three qubit quantum gates, users had to use many quantum gates to apply only one single CNOT gate [(see the Fig. 2a], SWAP gate or other two qubit and three-qubit quantum gates which are shown in Fig. 2 as an examples.

In paper [14], the obtained results has been shown that if we increase the number of gates in the circuit in the IBM quantum computer then the fidelity falls rapidly. To prove this point, why fidelity decreases to increase the number of gates on the qubit lines?, in this paper [22], a quantum process tomography has been performed for all single qubit quantum gates and two-qubit CNOT gate and calculated that which quantum gate has how much error. And also studied that to make a scalable SQUID-based quantum computer, errors introduced by the gates (in the present technology) have to be reduced considerably. But now, we have the user's friendly newest version (In the newest version [33], several quantum gates are added, like two-qubit SWAP gate, unitary

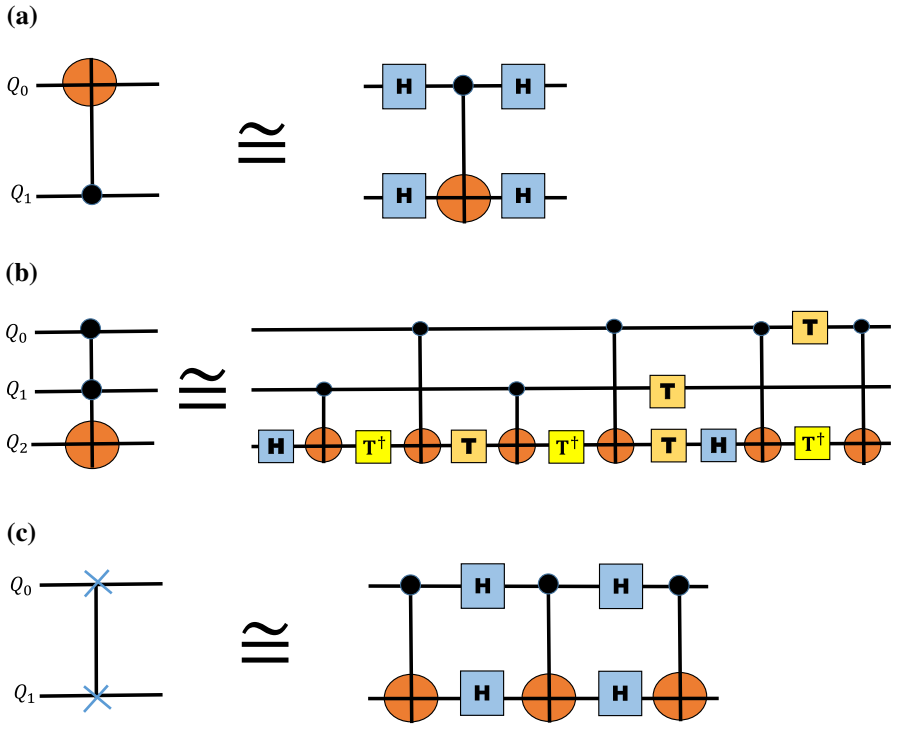

Fig. 2 Schematic diagrams of two and three qubit quantum gates in IBM quantum computer. **a** Q_0 is target and Q_1 is control, but according to the above (shown in Fig. 1) topology, it cannot be applied directly, so it has to be create by using four Hadamard and one CNOT gate (Q_0 is control and Q_1 is target). Due to unavailability of three-qubit quantum gate, like Toffoli and two qubit, like SWAP quantum gates in IBM quantum processor, **b** is the creation of Toffoli gate and **c** is the creation of a SWAP gate by using four Hadamard and three CNOT gates

operations to create any gate, three-qubit Toffoli gate) of IBMQX2 and IBMQX4 five-qubit IBM quantum computers, which has launched by IBM Corporation in 2019 [33], as well as the other new five-qubit quantum computers also launched i.e. IBM_ourense, IBM_vigo, IBM_essex etc [33]. The comparison performance between these newest five-qubit IBM quantum computers (IBM_ourense, IBM_vigo, IBMQX2, IBMQX4) have not yet been realized. Keeping this point in mind, in this paper, we have compared the performance of these newest IBM five-qubit quantum computers to analyze that which one gives better results in terms of fidelity for the Bell states.

The paper is organized as follows. In Sect. 2, we have prepared all four Bell states on different five-qubit IBM quantum computers (2.1–2.4). In Sect. 3, we have shown the results in Table 1. Finally, the paper is concluded in Sect.4.

Table 1 This table shows the fidelity of all Bell states on different five-qubit IBM quantum computers. The experimental results are obtained by running the each experiment with 8192 number of shots

Bell states	IBM_ourense	IBM_vigo	IBMQX2	IBMQX4
$\|\psi^+\rangle$	0.966	0.962	0.904	0.814
$\|\psi^-\rangle$	0.965	0.955	0.947	0.892
$\|\phi^+\rangle$	0.963	0.956	0.950	0.884
$\|\phi^-\rangle$	0.965	0.946	0.837	0.828

2 Bell states preparation on IBM quantum computers

Entangled states play a very important role in the field of quantum computation and quantum information [34]. Highly entangled states like Bell states, GHZ states and cluster states has been used to performed the quantum information processing tasks such as quantum teleportation [14,32,35–40], quantum secret sharing [32,40–43], quantum information splitting [32,41,44–46], quantum cheque [47], super dense coding [32,44,48] etc. In this paper, we have discussed only for Bell states. There are four Bell states which can be written as

$$\begin{aligned} |\psi^+\rangle &= \frac{|00\rangle+|11\rangle}{\sqrt{2}} \\ |\psi^-\rangle &= \frac{|00\rangle-|11\rangle}{\sqrt{2}} \\ |\phi^+\rangle &= \frac{|01\rangle+|10\rangle}{\sqrt{2}} \\ |\phi^-\rangle &= \frac{|01\rangle-|10\rangle}{\sqrt{2}} \end{aligned} \tag{1}$$

Bell state $|\psi^+\rangle$ prepares by using single and two-qubit quantum gate, i.e., Hadamard (H) gate followed by CNOT gate, which generate the maximally entangled state $\frac{|00\rangle+|11\rangle}{\sqrt{2}}$ (see the circuit shown in Fig. 3). The mathematical operation of this circuit is CNOT$(H \otimes I)\,|00\rangle$. We start with two separable states $|0\rangle \otimes |0\rangle$. Now, first of all H applied on the first qubit and I on the second qubit. Subsequently, CNOT operates on it, where the first qubit works as control qubit and the second qubit works as target qubit. According to the CNOT gate, second qubit will be flip when the first qubit is $|1\rangle$. Finally, the state is $\frac{|00\rangle+|11\rangle}{\sqrt{2}}$. Similarly, other Bell states $|\psi^-\rangle$, $|\phi^+\rangle$ and $|\phi^-\rangle$ can also be prepared by using some single and two-qubit quantum gates, which are shown in Fig. 3.

In this section, we have reconstructed experimental density matrices by using quantum state tomography all four Bell states on the IBM_ourense, IBM_vigo, IBMQX2, IBMQX4 IBM quantum computers as shown in below sections (2.1–2.4).

2.1 IBM_ourense

IBM_ourense is the newest five-qubit IBM quantum computer which is placed in the cloud in 2019 by IBM Corporation. Architecture of IBM_ourense as shown in Fig. 4. We have prepared all four Bell states (as shown in Fig. 3, same gates have been

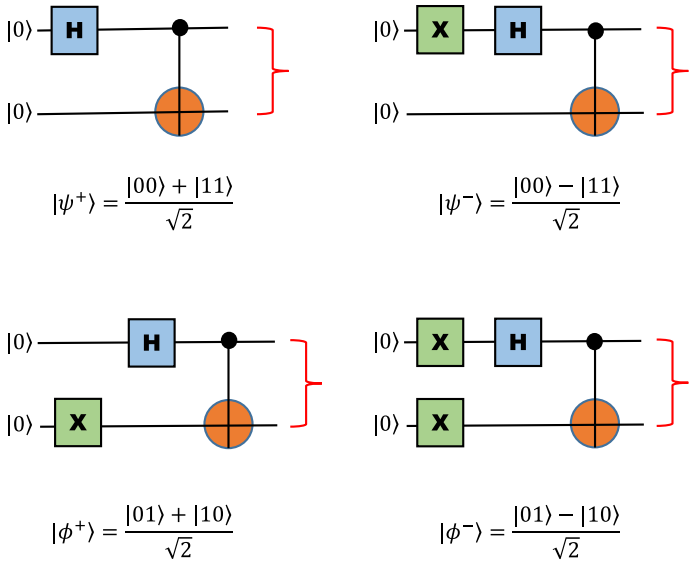

Fig. 3 Quantum circuits for Bell states preparation by using quantum gates. It transforms a separable input states $|00\rangle$ to a different maximally entangled Bell states as shown

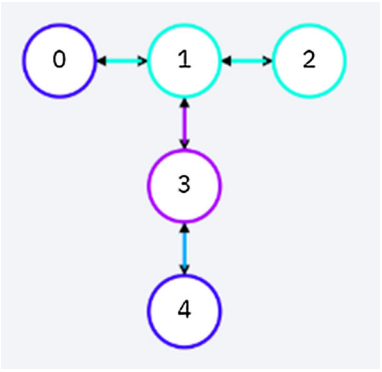

Fig. 4 Architecture of IBM_ourense

used as well as Z basis measurement was also performed to get the each element of density matrices) in the IBM_ourense quantum computer. We have reconstructed density matrices for all Bell states using quantum state tomography by following the method adopted in Refs. [10,14,22,37,49,50]. The proper details of reconstruction of 4×4 density matrix of 2-qubit quantum state (Bell states) are provided in Refs. [14,37].

The theoretical density matrix of the initially prepared Bell state $|\psi^+\rangle$ is given by,

$$\rho^{\mathrm{T}} = |\psi^+\rangle\langle\psi^+| \tag{2}$$

where superscript "T" indicates the theoretical density matrix and the expression of the experimental density matrix for two-qubit quantum system is represented as,

$$\rho^{\mathrm{E}} = \frac{1}{4}\sum_{i,j} \prec \sigma_i \otimes \sigma_j \succ \sigma_i \otimes \sigma_j \tag{3}$$

where, $\sigma_{i,j}$ is the I, X, Y, Z and superscript "E" indicates the experimental density matrix.

Density matrix for the experimentally obtained state corresponding to a particular case $|\psi^+\rangle$, is obtained as

$$\rho^{\mathrm{E}} = \mathrm{Re}\left[\rho^{\mathrm{E}}_{|\psi^+\rangle}\right] + i\ \mathrm{Im}\left[\rho^{\mathrm{E}}_{|\psi^+\rangle}\right] \tag{4}$$

$$\mathrm{Re}\left[\rho^{\mathrm{E}}_{|\psi^+\rangle}\right] = \begin{pmatrix} 0.423 & 0.009 & -0.009 & 0.448 \\ 0.009 & 0.022 & 0.006 & 0.016 \\ -0.009 & 0.006 & 0.026 & -0.010 \\ 0.447 & 0.016 & -0.010 & 0.530 \end{pmatrix} \tag{5}$$

$$\mathrm{Im}\left[\rho^{\mathrm{E}}_{|\psi^+\rangle}\right] = \begin{pmatrix} 0 & -0.009 & 0.001 & -0.002 \\ 0.009 & 0 & -0.002 & -0.006 \\ -0.001 & 0.002 & 0 & -0.009 \\ 0.002 & 0.006 & 0.009 & 0 \end{pmatrix} \tag{6}$$

Real part of this density matrix is illustrated in Fig. 5. Figure 5 also illustrates the real part of density matrices of the experimentally prepared other Bell states $|\psi^-\rangle$, $|\phi^+\rangle$ and $|\phi^-\rangle$. Corresponding density matrices are provided in "Appendix" (see Eq. (19–24)).

2.2 IBM_vigo

IBM_vigo is the newest five-qubit IBM quantum computer which is placed in the cloud in 2019 by IBM Corporation. Architecture of IBM_vigo as shown in Fig. 6. Similarly, we have prepared all four Bell states in IBM_vigo.

The theoretical density matrix of the initially prepared Bell state $|\psi^-\rangle$ is given by,

$$\rho^{\mathrm{T}} = |\psi^-\rangle\langle\psi^-| \tag{7}$$

Density matrix for the experimentally obtained state corresponding to a particular case $|\psi^-\rangle$, is obtained as

$$\rho^{\mathrm{E}} = \mathrm{Re}\left[\rho^{E}_{|\psi^-\rangle}\right] + i\ \mathrm{Im}\left[\rho^{E}_{|\psi^-\rangle}\right] \tag{8}$$

$$\mathrm{Re}\left[\rho^{\mathrm{E}}_{|\psi^-\rangle}\right] = \begin{pmatrix} 0.496 & 0.014 & 0.008 & -0.445 \\ 0.014 & 0.036 & -0.019 & -0.017 \\ 0.008 & -0.019 & 0.027 & 0.005 \\ -0.445 & -0.017 & 0.005 & 0.440 \end{pmatrix} \tag{9}$$

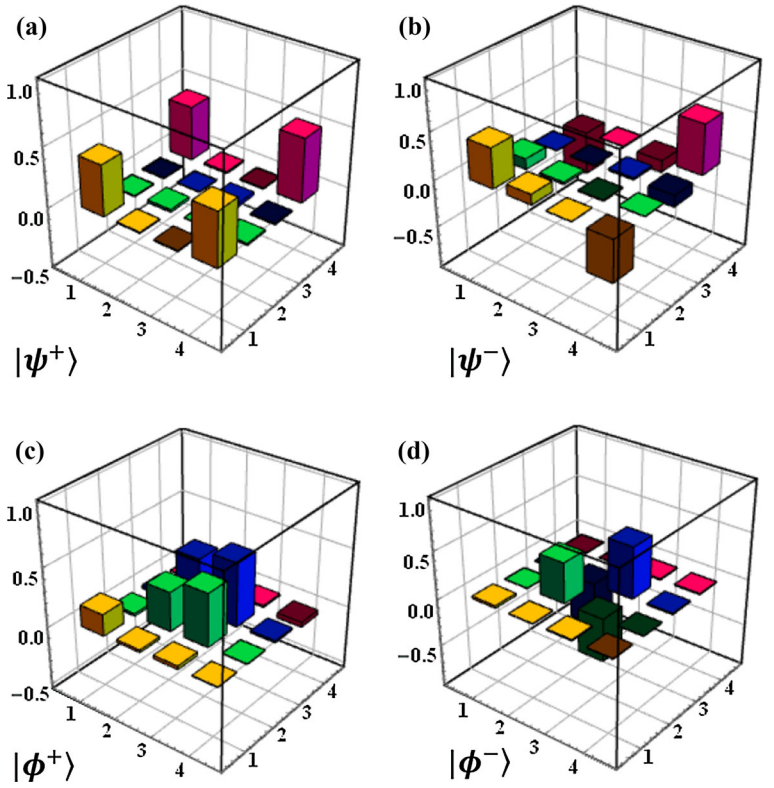

Fig. 5 Reconstructed Bell states corresponding to ideal states (a) $|\psi^+\rangle$, (b) $|\psi^-\rangle$, (c) $|\phi^+\rangle$, and (d) $|\phi^-\rangle$. In each plot of the figure, the states $|00\rangle$, $|01\rangle$, $|10\rangle$ and $|11\rangle$ are labeled as 1–4 consecutively in X and Y axis

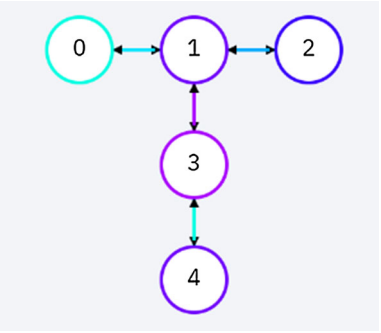

Fig. 6 Architecture of five-qubit IBM_vigo quantum computer

$$\mathrm{Im}\left[\rho^{\mathrm{E}}_{|\psi^-\rangle}\right] = \begin{pmatrix} 0 & 0.024 & -0.033 & -0.034 \\ -0.024 & 0 & -0.005 & 0.021 \\ 0.033 & 0.005 & 0 & -0.024 \\ 0.034 & -0.021 & 0.024 & 0 \end{pmatrix} \tag{10}$$

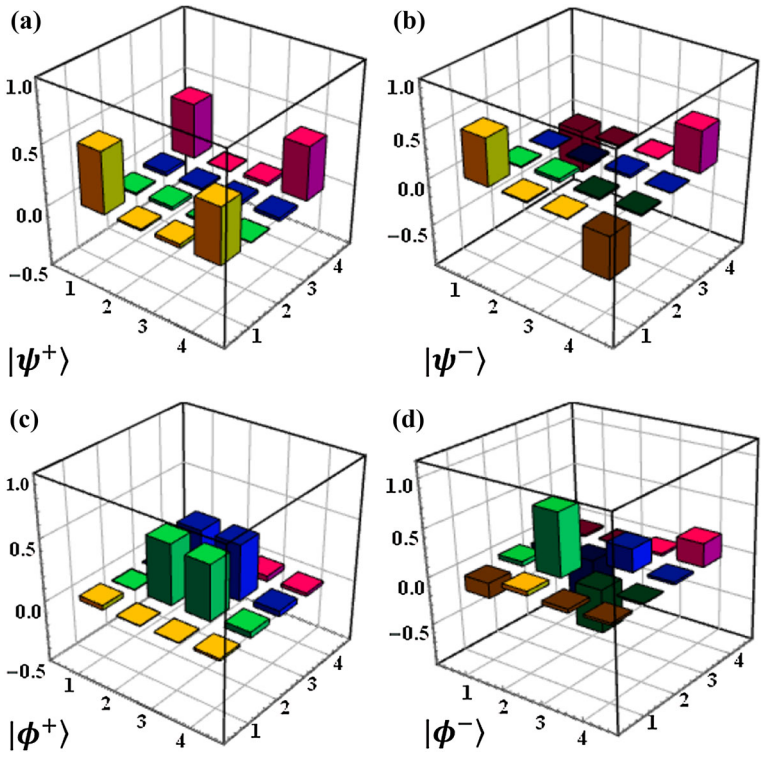

Fig. 7 Graphical representation of real part of reconstructed density matrices of Bell states corresponding to ideal states (a) $|\psi^+\rangle$, (b) $|\psi^-\rangle$, (c) $|\phi^+\rangle$, and (d) $|\phi^-\rangle$. In each plot of the figure, the states $|00\rangle$, $|01\rangle$, $|10\rangle$ and $|11\rangle$ are labeled as 1–4 consecutively in X and Y axis

Figure 7 illustrates real part of density matrices of the experimentally prepared all Bell states $|\psi^+\rangle$, $|\psi^-\rangle$, $|\phi^+\rangle$ and $|\phi^-\rangle$. Corresponding density matrices for Bell states $|\psi^+\rangle$, $|\phi^+\rangle$ and $|\phi^-\rangle$ are provided in Appendix [(see Eq. (25–30)].

2.3 IBMQX2

IBMQX2 is the new version of old IBMQX2 version with the lots of advantage as comparison to old. In Fig. 8, architecture of IBMQ2 has shown. Similarly, we have prepared all four Bell states in IBMQX2.

The theoretical density matrix of the initially prepared Bell state $|\phi^+\rangle$ is given by,

$$\rho^{\mathrm{T}} = |\phi^+\rangle\langle\phi^+| \tag{11}$$

Density matrix for the experimentally obtained state corresponding to a particular case $|\phi^+\rangle$, is obtained as

$$\rho^{\mathrm{E}} = \mathrm{Re}\left[\rho^{\mathrm{E}}_{|\phi^+\rangle}\right] + i\ \mathrm{Im}\left[\rho^{\mathrm{E}}_{|\phi^+\rangle}\right] \tag{12}$$

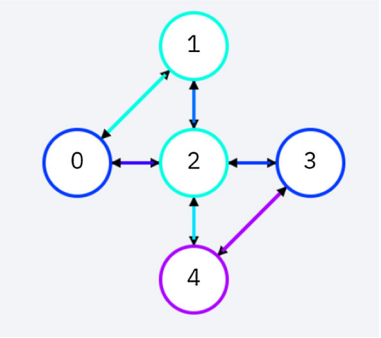

Fig. 8 Architecture of new version of IBMQX2

$$\mathrm{Re}\left[\rho^{\mathrm{E}}_{|\phi^+\rangle}\right] = \begin{pmatrix} 0.027 & 0.045 & 0.004 & 0.002 \\ 0.045 & 0.319 & 0.468 & -0.066 \\ 0.004 & 0.468 & 0.552 & -0.023 \\ 0.002 & -0.066 & -0.023 & 0.099 \end{pmatrix} \tag{13}$$

$$\mathrm{Im}\left[\rho^{\mathrm{E}}_{|\phi^+\rangle}\right] = \begin{pmatrix} 0 & 0.002 & 0.046 & -0.059 \\ -0.002 & 0 & -0.039 & 0.048 \\ 0.046 & 0.039 & 0 & -0.006 \\ 0.059 & -0.048 & 0.006 & 0 \end{pmatrix} \tag{14}$$

Figure 9 illustrates real part of density matrices of the experimentally prepared all Bell states $|\psi^+\rangle$, $|\psi^-\rangle$, $|\phi^+\rangle$and $|\phi^-\rangle$. Corresponding density matrices for Bell states $|\psi^+\rangle$, $|\phi^+\rangle$ and $|\phi^-\rangle$ are provided in "Appendix" [(see Eq. (31–35)].

2.4 IBMQX4

IBMQX4 is the user's friendly newest version of old IBMQX4 quantum computer. In Fig. 10, architecture of IBMQ4 has shown. Same the above, we have prepared all four Bell states in IBMQX4.

The theoretical density matrix of the initially prepared Bell state $|\phi^-\rangle$ is given by,

$$\rho^{\mathrm{T}} = |\phi^-\rangle\langle\phi^-| \tag{15}$$

Density matrix for the experimentally obtained state corresponding to a particular case $|\phi^-\rangle$, is obtained as

$$\rho^{\mathrm{E}} = \mathrm{Re}\left[\rho^{\mathrm{E}}_{|\phi^-\rangle}\right] + i\ \mathrm{Im}\left[\rho^{\mathrm{E}}_{|\phi^-\rangle}\right] \tag{16}$$

$$\mathrm{Re}\left[\rho^{\mathrm{E}}_{|\phi^-\rangle}\right] = \begin{pmatrix} 0.189 & 0.041 & 0.127 & -0.001 \\ 0.042 & 0.458 & -0.288 & 0.073 \\ 0.127 & -0.288 & 0.337 & 0.026 \\ -0.001 & 0.073 & 0.026 & 0.017 \end{pmatrix} \tag{17}$$

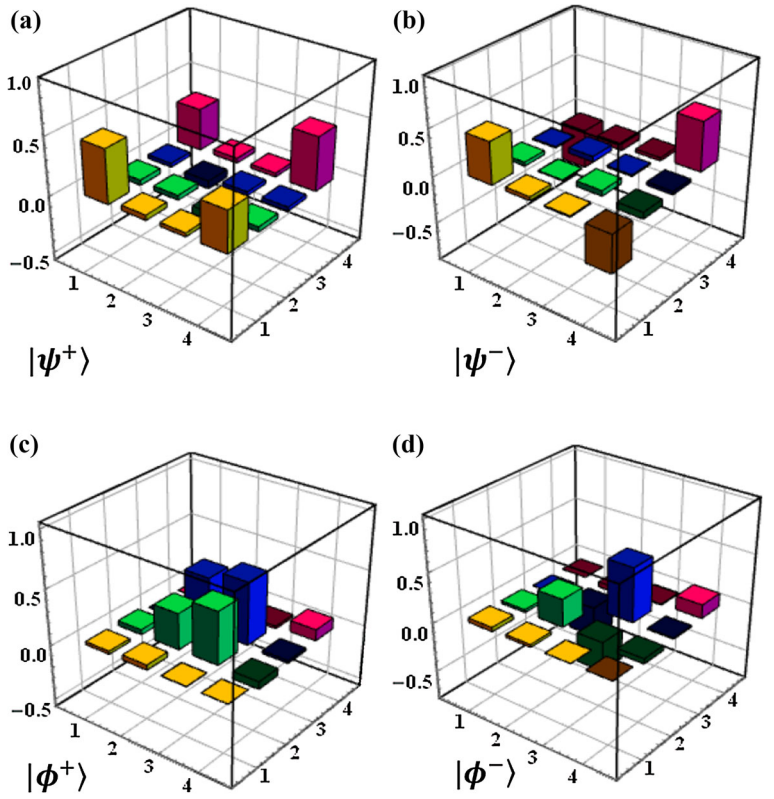

Fig. 9 Reconstructed density matrices of Bell states corresponding to ideal states (a) $|\psi^+\rangle$, (b) $|\psi^-\rangle$, (c) $|\phi^+\rangle$, and (d) $|\phi^-\rangle$. The states $|00\rangle$, $|01\rangle$, $|10\rangle$ and $|11\rangle$ are labeled as 1–4 consecutively in X and Y axis in each plot of the Figure

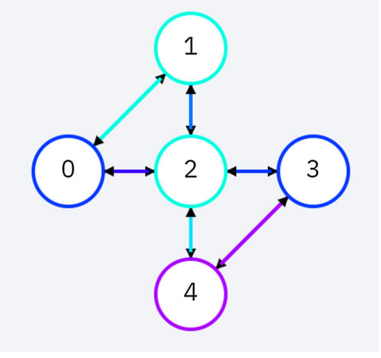

Fig. 10 Architecture of new version of five-qubit IBMQX4

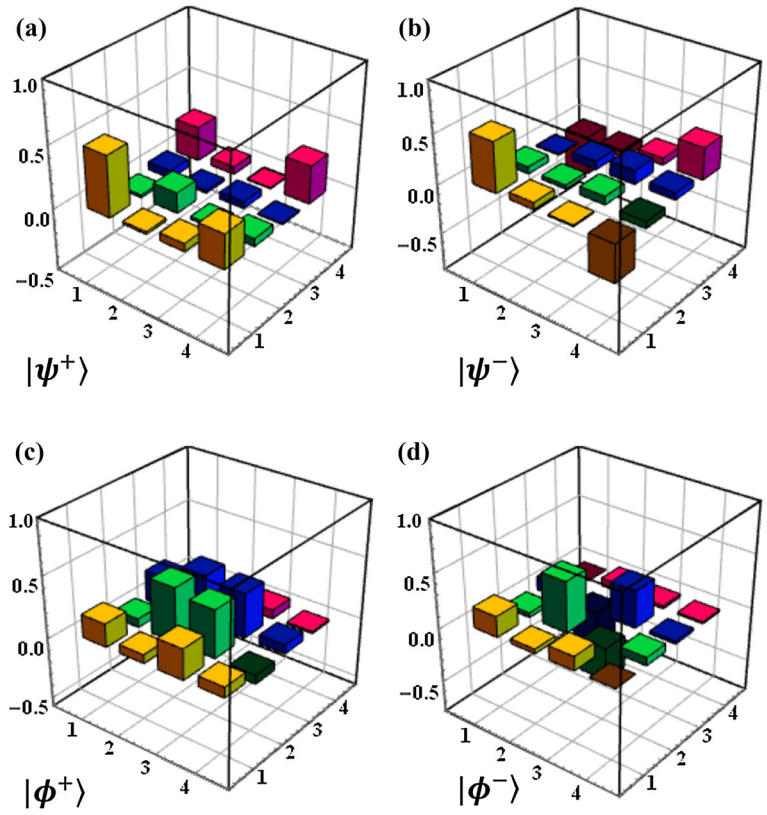

Fig. 11 Experimentally reconstructed density matrices of all Bell states corresponding to ideal states (a) $|\psi^+\rangle$, (b) $|\psi^-\rangle$, (c) $|\phi^+\rangle$, and (d) $|\phi^-\rangle$ on IBMQX4 quantum computer. The states $|00\rangle$, $|01\rangle$, $|10\rangle$ and $|11\rangle$ are labeled as 1–4 consecutively in X and Y axis in each plot of the Figure

$$\mathrm{Im}\left[\rho^{\mathrm{E}}_{|\phi^-\rangle}\right] = \begin{pmatrix} 0 & 0.051 & -0.066 & -0.023 \\ -0.051 & 0 & -0.002 & -0.061 \\ 0.066 & 0.003 & 0 & 0.077 \\ 0.023 & 0.061 & -0.077 & 0 \end{pmatrix} \tag{18}$$

Various real elements of all the density matrices for all Bell states are shown pictorially in Fig. 11. Corresponding density matrices for Bell states $|\psi^+\rangle$, $|\psi^-\rangle$ and $|\phi^+\rangle$ are provided in "Appendix" [(see Eq. (36–41)].

3 Results

In the above Sect. (2.1–2.4), we have reconstructed experimental density matrices for all Bell states on different IBM quantum computers. In this section, a table of fidelity for all Bell states for four IBM quantum computers IBM_ourense, IBM_vigo, IBMQX2, IBMQX4 have shown. Fidelity are calculated between the experimentally observed and theoretically density matrix by using the formula $F = \mathrm{Tr}\sqrt{\sqrt{\rho_1}\rho_2\sqrt{\rho_1}}$

[51], where $\rho_1 = \rho^{\mathrm{T}}$theoretical density matrix and $\rho_2 = \rho^{\mathrm{E}}$ experimentally obtained density matrix.

4 Conclusion

We performed analysis of different quantum computing platforms available on cloud by IBM as far as Bell state preparation is concerned. As the Bell state generation requires at least a single qubit Hadamard and a CNOT gate, this choice of state preparation for comparative performance is a preferred candidate. Specifically, we have compared the performance of four superconductivity-based IBM quantum computers, i.e. IBM_ourense, IBM_vigo, IBMQX2, IBMQX4. To compare the performance between these IBM quantum computers, we have prepared all four Bell states on it and obtained the fidelity between experimentally reconstructed and theoretical density matrices. This comparison revealed that IBM_ourense quantum computer yields better fidelity than others (IBM_vigo, IBMQX2, IBMQX4), and IBMQX4 gives worse fidelity for all the Bell states. We can also write the obtained fidelity for these (IBM_ourense, IBM_vigo, IBMQX2, IBMQX4) IBM quantum computers in the descending order of performance $F_{IBM\_ourense} \succ F_{IBM\_vigo} \succ F_{IBMQX2} \succ F_{IBMQX4}$. The present results are consistent with some of our recent studies [14].

We hope the present study will help in identifying the scope of improvement and suggest preferred choice of quantum computing platform for performing quantum computing and simulation experiments.

Acknowledgements MS thanks the Department of Science and Technology (DST), India, for support provided through the DST project No. S/DST/VNA/20190004. MS also gratefully thanks to Kishore Thapliyal for some fruitful discussions and suggestions.

Appendix: Experimentally obtained density matrices for Bell states on IBM_ourense

$$\mathrm{Re}\left[\rho^{\mathrm{E}}_{|\psi^-\rangle}\right] = \begin{pmatrix} 0.422 & 0.110 & 0.004 & -0.453 \\ 0.110 & 0.024 & -0.010 & 0.005 \\ 0.004 & -0.010 & 0.021 & -0.122 \\ -0.453 & 0.005 & -0.122 & 0.532 \end{pmatrix} \tag{19}$$

$$\mathrm{Im}\left[\rho^{\mathrm{E}}_{|\psi^-\rangle}\right] = \begin{pmatrix} 0 & -0.012 & 0.002 & -0.012 \\ 0.012 & 0 & -0.001 & -0.014 \\ 0.002 & 0.001 & 0 & 0.004 \\ 0.012 & 0.014 & -0.004 & 0 \end{pmatrix} \tag{20}$$

$$\mathrm{Re}\left[\rho^{\mathrm{E}}_{|\phi^+\rangle}\right] = \begin{pmatrix} 0.182 & 0.022 & 0.030 & 0.005 \\ 0.022 & 0.328 & 0.447 & 0.006 \\ 0.030 & 0.447 & 0.532 & 0.017 \\ 0.005 & 0.006 & 0.017 & -0.042 \end{pmatrix} \tag{21}$$

$$\mathrm{Im}\left[\rho^{\mathrm{E}}_{|\phi^{+}\rangle}\right] = \begin{pmatrix} 0 & -0.001 & -0.012 & 0.003 \\ 0.001 & 0 & -0.072 & -0.011 \\ 0.012 & 0.072 & 0 & -0.009 \\ -0.003 & 0.011 & 0.009 & 0 \end{pmatrix} \tag{22}$$

$$\mathrm{Re}\left[\rho^{\mathrm{E}}_{|\phi^{-}\rangle}\right] = \begin{pmatrix} 0.026 & 0.006 & 0.013 & -0.008 \\ 0.006 & 0.422 & -0.449 & -0.005 \\ 0.013 & -0.449 & 0.540 & 0.014 \\ -0.009 & -0.005 & 0.014 & 0.012 \end{pmatrix} \tag{23}$$

$$\mathrm{Im}\left[\rho^{\mathrm{E}}_{|\phi^{-}\rangle}\right] = \begin{pmatrix} 0 & -0.003 & -0.011 & 0.007 \\ 0.003 & 0 & 0.074 & 0.014 \\ 0.011 & -0.0746 & 0 & -0.023 \\ -0.007 & -0.014 & 0.023 & 0 \end{pmatrix} \tag{24}$$

Experimentally obtained density matrices for Bell states on IBM_vigo

$$\mathrm{Re}\left[\rho^{\mathrm{E}}_{|\psi^{+}\rangle}\right] = \begin{pmatrix} 0.505 & 0.015 & 0.030 & 0.453 \\ 0.015 & 0.027 & 0.017 & 0.006 \\ 0.030 & 0.017 & 0.026 & 0.027 \\ 0.453 & 0.006 & 0.027 & 0.442 \end{pmatrix} \tag{25}$$

$$\mathrm{Im}\left[\rho^{\mathrm{E}}_{|\psi^{+}\rangle}\right] = \begin{pmatrix} 0 & 0.006 & 0.009 & 0.024 \\ -0.006 & 0 & -0.001 & -0.009 \\ -0.009 & 0.001 & 0 & -0.018 \\ -0.024 & 0.009 & 0.018 & 0 \end{pmatrix} \tag{26}$$

$$\mathrm{Re}\left[\rho^{\mathrm{E}}_{|\phi^{+}\rangle}\right] = \begin{pmatrix} 0.038 & 0.005 & 0.006 & 0.018 \\ 0.005 & 0.488 & 0.447 & 0.047 \\ 0.006 & 0.447 & 0.446 & 0.045 \\ 0.018 & 0.047 & 0.045 & 0.027 \end{pmatrix} \tag{27}$$

$$\mathrm{Im}\left[\rho^{\mathrm{E}}_{|\phi^{+}\rangle}\right] = \begin{pmatrix} 0 & -0.001 & -0.007 & 0.001 \\ 0.001 & 0 & 0.030 & 0.002 \\ 0.007 & -0.030 & 0 & 0.003 \\ -0.001 & -0.002 & -0.003 & 0 \end{pmatrix} \tag{28}$$

$$\mathrm{Re}\left[\rho^{\mathrm{E}}_{|\phi^{-}\rangle}\right] = \begin{pmatrix} -0.154 & 0.047 & -0.039 & -0.023 \\ 0.047 & 0.669 & -0.439 & -0.007 \\ -0.039 & -0.439 & 0.243 & 0.024 \\ -0.023 & -0.007 & 0.024 & 0.243 \end{pmatrix} \tag{29}$$

$$\mathrm{Im}\left[\rho^{\mathrm{E}}_{|\phi^{-}\rangle}\right] = \begin{pmatrix} 0 & -0.032 & 0.022 & 0.001 \\ 0.032 & 0 & -0.048 & -0.037 \\ -0.022 & 0.048 & 0 & 0.025 \\ -0.001 & 0.037 & -0.025 & 0 \end{pmatrix} \tag{30}$$

Experimentally obtained density matrices for Bell states on IBMQX2

$$\mathrm{Re}\left[\rho^{\mathrm{E}}_{|\psi^+\rangle}\right] = \begin{pmatrix} 0.465 & 0.044 & 0.033 & 0.354 \\ 0.044 & 0.041 & -0.066 & 0.042 \\ 0.033 & -0.066 & 0.034 & 0.033 \\ 0.354 & 0.042 & 0.033 & 0.459 \end{pmatrix} \tag{31}$$

$$\mathrm{Im}\left[\rho^{\mathrm{E}}_{|\psi^+\rangle}\right] = \begin{pmatrix} 0 & 0.004 & 0.009 & 0.009 \\ 0.004 & 0 & -0.001 & -0.004 \\ 0.009 & 0.001 & 0 & 0.001 \\ 0.009 & 0.004 & -0.001 & 0 \end{pmatrix} \tag{32}$$

$$\mathrm{Re}\left[\rho^{\mathrm{E}}_{|\psi^-\rangle}\right] = \begin{pmatrix} 0.448 & 0.041 & 0.013 & -0.411 \\ 0.041 & 0.009 & 0.057 & -0.070 \\ 0.013 & 0.057 & 0.015 & -0.034 \\ -0.411 & -0.070 & -0.034 & 0.525 \end{pmatrix} \tag{33}$$

$$\mathrm{Im}\left[\rho^{\mathrm{E}}_{|\psi^-\rangle}\right] = \begin{pmatrix} 0 & -0.058 & 0.028 & -0.067 \\ 0.058 & 0 & 0.007 & 0.056 \\ -0.028 & -0.007 & 0 & 0.038 \\ 0.067 & -0.056 & -0.038 & 0 \end{pmatrix} \tag{34}$$

$$\mathrm{Re}\left[\rho^{\mathrm{E}}_{|\phi^-\rangle}\right] = \begin{pmatrix} 0.043 & 0.028 & 0.002 & -0.001 \\ 0.028 & 0.277 & -0.290 & -0.050 \\ 0.002 & -0.290 & 0.543 & -0.010 \\ -0.001 & -0.050 & -0.010 & 0.136 \end{pmatrix} \tag{35}$$

$$\mathrm{Im}\left[\rho^{\mathrm{E}}_{|\phi^-\rangle}\right] = \begin{pmatrix} 0 & 0.030 & 0.005 & -0.047 \\ 0.030 & 0 & 0.023 & 0.060 \\ 0.005 & 0.023 & 0 & -0.003 \\ 0.047 & -0.060 & 0.003 & 0 \end{pmatrix}$$

Experimentally obtained density matrices for Bell states on IBMQX4

$$\mathrm{Re}\left[\rho^{\mathrm{E}}_{|\psi^+\rangle}\right] = \begin{pmatrix} 0.484 & 0.021 & 0.063 & 0.271 \\ 0.021 & 0.161 & 0.022 & 0.062 \\ 0.063 & 0.022 & 0.053 & 0.007 \\ 0.271 & 0.062 & 0.007 & 0.299 \end{pmatrix} \tag{36}$$

$$\mathrm{Im}\left[\rho^{\mathrm{E}}_{|\psi^+\rangle}\right] = \begin{pmatrix} 0 & -0.024 & -0.078 & 0.010 \\ 0.024 & 0 & 0.001 & -0.069 \\ 0.078 & 0.001 & 0 & -0.011 \\ -0.010 & 0.069 & 0.011 & 0 \end{pmatrix} \tag{37}$$

$$\mathrm{Re}\left[\rho^{\mathrm{E}}_{|\psi^-\rangle}\right] = \begin{pmatrix} 0.504 & 0.070 & 0.013 & -0.384 \\ 0.070 & 0.038 & 0.084 & -0.070 \\ 0.013 & 0.084 & 0.138 & 0.072 \\ -0.384 & -0.070 & 0.072 & 0.319 \end{pmatrix} \tag{38}$$

$$\mathrm{Im}\left[\rho^{\mathrm{E}}_{|\psi^-\rangle}\right] = \begin{pmatrix} 0 & -0.079 & -0.020 & -0.011 \\ 0.079 & 0 & 0.013 & -0.017 \\ 0.020 & -0.013 & 0 & -0.072 \\ 0.011 & 0.018 & 0.072 & 0 \end{pmatrix} \tag{39}$$

$$\mathrm{Re}\left[\rho^{\mathrm{E}}_{|\phi^+\rangle}\right] = \begin{pmatrix} 0.188 & 0.070 & 0.246 & 0.086 \\ 0.070 & 0.438 & 0.384 & -0.071 \\ 0.246 & 0.385 & 0.357 & 0.072 \\ 0.086 & -0.071 & 0.072 & 0.016 \end{pmatrix} \tag{40}$$

$$\mathrm{Im}\left[\rho^{\mathrm{E}}_{|\phi^+\rangle}\right] = \begin{pmatrix} 0 & -0.017 & -0.076 & -0.006 \\ 0.017 & 0 & -0.023 & -0.066 \\ 0.076 & 0.023 & 0 & -0.011 \\ 0.006 & 0.067 & 0.012 & 0 \end{pmatrix} \tag{41}$$

References

1. Hou, S.-Y., Sheng, Y.-B., Feng, G.-R., Long, G.-L.: Experimental optimal single qubit purification in an NMR quantum information processor. Sci. Rep. **4**, 6857 (2014)
2. Laflamme, R., Cory, D. G., Negrevergne, C., Viola, L.: NMR quantum information processing and entanglement. arXiv preprint arXiv:quant-ph/0110029 (2001)
3. Samal, J.R., Gupta, M., Panigrahi, P., Kumar, A.: Non-destructive discrimination of bell states by NMR using a single ancilla qubit. J. Phys. B Atomic Mol. Opt. Phys. **43**, 095508 (2010)
4. Ma, C., Sacher, W.D., Tang, Z., et al.: Silicon photonic transmitter for polarization-encoded quantum key distribution. Optica **3**, 1274–1278 (2016)
5. Zhang, G., Haw, J., Cai, H., et al.: An integrated silicon photonic chip platform for continuous-variable quantum key distribution. Nature Photonics **13**, 839–842 (2019)
6. Sheng, Y., Liu, J., Zhao, S., Zhou, L.: Multipartite entanglement concentration for nitrogen-vacancy center and microtoroidal resonator system. Chin. Sci. Bull. **58**, 3507–3513 (2013)
7. Riebe, M., Monz, T., Kim, K., et al.: Deterministic entanglement swapping with an ion-trap quantum computer. Nature Phys. **4**, 839 (2008)
8. Barrett, M., Chiaverini, J., Schaetz, T., et al.: Deterministic quantum teleportation of atomic qubits. Nature **429**, 737 (2004)
9. IBM quantum computing platform. platform (2016). http://research.ibm.com/ibm-q/qx/. Accessed 4 May 2016
10. Alsina, D., Latorre, J.I.: Experimental test of mermin inequalities on a five-qubit quantum computer. Phys. Rev. A **94**, 012314 (2016)
11. Behera, B.K., Banerjee, A., Panigrahi, P.K.: Experimental realization of quantum cheque using a five-qubit quantum computer. Quantum Inf. Process. **16**, 312 (2017)
12. Hebenstreit, M., Alsina, D., Latorre, J., Kraus, B.: Compressed quantum computation using a remote five-qubit quantum computer. Phys. Rev. A **95**, 052339 (2017)
13. Majumder, A., Mohapatra, S., Kumar, A.: Experimental realization of secure multiparty quantum summation using five-qubit IBM quantum computer on cloud. arXiv preprint arXiv:1707.07460 (2017)
14. Sisodia, M., Shukla, A., Pathak, A.: Experimental realization of nondestructive discrimination of bell states using a five-qubit quantum computer. Phys. Lett. A **381**, 3860–3874 (2017)
15. Wootton, J.R.: Demonstrating non-abelian braiding of surface code defects in a five qubit experiment. Quantum Sci. Technol. **2**, 015006 (2017)

16. Behera, B.K., Seth, S., Das, A., Panigrahi, P.K.: Demonstration of entanglement purification and swapping protocol to design quantum repeater in IBM quantum computer. Quantum Inf. Process. **18**, 108 (2019)
17. Behera, B.K., Reza, T., Gupta, A., Panigrahi, P.K.: Designing quantum router in IBM quantum computer. Quantum Inf. Process. **18**, 328 (2019)
18. Ferrari, D., Amoretti, M.: Demonstration of envariance and parity learning on the IBM 16 qubit processor. arXiv preprint arXiv:1801.02363 (2018)
19. Ghosh, D., Agarwal, P., Pandey, P., Behera, B.K., Panigrahi, P.K.: Automated error correction in IBM quantum computer and explicit generalization. Quantum Inf. Process. **17**, 153 (2018)
20. Kalra, A.R., Gupta, N., Behera, B.K., Prakash, S., Panigrahi, P.K.: Demonstration of the no-hiding theorem on the 5-qubit IBM quantum computer in a category-theoretic framework. Quantum Inf. Process. **18**, 170 (2019)
21. Pathak, A.: Experimental quantum mechanics in the class room: testing basic ideas of quantum mechanics and quantum computing using IBM quantum computer. arXiv preprint arXiv:1805.06275 (2018)
22. Shukla, A., Sisodia, M., Pathak, A.: Complete characterization of the directly implementable quantum gates used in the IBM quantum processors. arXiv preprint arXiv:1805.07185 (2018)
23. Singh, R. K., Panda, B., Behera, B. K., Panigrahi, P. K.: Demonstration of a general fault-tolerant quantum error detection code for (2n+1)-qubit entangled state on IBM 16-qubit quantum computer. arXiv preprint arXiv:1807.02883 (2018)
24. Sisodia, M., Shukla, A., de Almeida, A. A., Dueck, G. W., Pathak, A.: Circuit optimization for IBM processors: A way to get higher fidelity and higher values of nonclassicality witnesses. arXiv preprint arXiv:1812.11602 (2018)
25. Wang, Y., Li, Y., Yin, Z.Q., Zeng, B.: 16-qubit IBM universal quantum computer can be fully entangled. npj Quantum Inf. **4**, 46 (2018)
26. Huffman, E., Mizel, A.: Violation of noninvasive macrorealism by a superconducting qubit: Implementation of a leggett-garg test that addresses the clumsiness loophole. Phys. Rev. A **95**, 032131 (2017)
27. Berta, M., Wehner, S., Wilde, M.M.: Entropic uncertainty and measurement reversibility. New J. Phys. **18**, 073004 (2016)
28. Das, S., Paul, G.: Experimental test of hardy's paradox on a five-qubit quantum computer. arXiv preprint arXiv:1712.04925 (2017)
29. Balu, R., Castillo, D., Siopsis, G.: Physical realization of topological quantum walks on IBM-q and beyond. Quantum Sci. Technol. **3**, 035001 (2018)
30. Yalçınkaya, İ., Gedik, Z.: Optimization and experimental realization of the quantum permutation algorithm. Phys. Rev. A **96**, 062339 (2017)
31. Deffner, S.: Demonstration of entanglement assisted invariance on IBM's quantum experience. Heliyon **3**, e00444 (2017)
32. Muralidharan, S., Panigrahi, P.K.: Perfect teleportation, quantum-state sharing, and superdense coding through a genuinely entangled five-qubit state. Phys. Rev. A **77**, 032321 (2008)
33. IBM quantum computing platform (2019). https://quantum-computing.ibm.com/
34. Nielson, M.A., Chuang, I.L.: Quantum computation and quantum information. Phys. Today **54**, 60–2 (2001)
35. Bennett, C.H., Brassard, G., Crépeau, C., et al.: Teleporting an unknown quantum state via dual classical and einstein-podolsky-rosen channels. Phys. Rev. Lett. **70**, 1895 (1993)
36. Ghosh, S., Kar, G., Roy, A., Sarkar, D., Sen, U.: Entanglement teleportation through ghz-class states. New J. Phys. **4**, 48 (2002)
37. Sisodia, M., Shukla, A., Thapliyal, K., Pathak, A.: Design and experimental realization of an optimal scheme for teleportation of an n-qubit quantum state. Quantum Inf. Process. **16**, 292 (2017)
38. Sisodia, M., Verma, V., Thapliyal, K., Pathak, A.: Teleportation of a qubit using entangled non-orthogonal states: a comparative study. Quantum Inf. Process. **16**, 76 (2017)
39. Sisodia, M., Pathak, A.: Comment on "quantum teleportation of eight-qubit state via six-qubit cluster state". Int. J. Theor. Phys. **57**, 2213–2217 (2018)
40. Choudhury, S., Muralidharan, S., Panigrahi, P.K.: Quantum teleportation and state sharing using a genuinely entangled six-qubit state. J. Phys. A Math. Theor. **42**, 115303 (2009)
41. Muralidharan, S., Karumanchi, S., Jain, S., Srikanth, R., Panigrahi, P.K.: 2n qubit "mirror states" for optimal quantum communication. Eur. Phys. J. D **61**, 757–763 (2011)

42. Jain, S., Muralidharan, S., Panigrahi, P.K.: Secure quantum conversation through non-destructive discrimination of highly entangled multipartite states. Euro. Phys. Lett. **87**, 60008 (2009)
43. Prasath, E.S., Muralidharan, S., Mitra, C., Panigrahi, P.K.: Multipartite entangled magnon states as quantum communication channels. Quantum Inf. Process. **11**, 397–410 (2012)
44. Paul, N., Menon, J.V., Karumanchi, S., Muralidharan, S., Panigrahi, P.K.: Quantum tasks using six qubit cluster states. Quantum Inf. Process. **10**, 619–632 (2011)
45. Panigrahi, P.K., Karumanchi, S., Muralidharan, S.: Minimal classical communication and measurement complexity for quantum information splitting of a two-qubit state. Pramana **73**, 499 (2009)
46. Muralidharan, S., Panigrahi, P.K.: Quantum-information splitting using multipartite cluster states. Phys. Rev. A **78**, 062333 (2008)
47. Moulick, S.R., Panigrahi, P.K.: Quantum cheques. Quantum Inf. Process. **15**, 2475–2486 (2016)
48. Agrawal, P., Pati, A.: Perfect teleportation and superdense coding with w states. Phys. Rev. A **74**, 062320 (2006)
49. Rundle, R., Tilma, T., Samson, J., Everitt, M.: Quantum state reconstruction made easy: a direct method for tomography. Phys. Rev. A **96**, 022117 (2017)
50. James, D.F., Kwiat, P.G., Munro, W.J., White, A.G.: On the measurement of qubits. In: Hayashi, M. (ed.) Asymptotic Theory of Quantum Statistical Inference: Selected Papers, pp. 509–538. World Scientific, Singapore (2005)
51. Pathak, A.: Elements of quantum computation and quantum communication. CRC Press, Boca Raton (2013)